ADVANCED MATERIALS

Supporting Information

Thin Film Thermoelectric Metal–Organic Framework with High Seebeck Coefficient and Low Thermal Conductivity

Kristopher J. Erickson, François Léonard, Vitalie Stavila, Michael E. Foster, Catalin D. Spataru, Reese E. Jones, Brian M. Foley, Patrick E. Hopkins, Mark D. Allendorf, and A. Alec Talin*

Supporting Information

Thin Film Thermoelectric Metal-Organic Framework with High Seebeck Coefficient and Low Thermal Conductivity

Kristopher J. Erickson, François Léonard, Vitalie Stavila, Michael E. Foster, Catalin D. Spataru, Reese E. Jones, Brian M. Foley, Patrick E. Hopkins, Mark D. Allendorf, and A. Alec Talin*
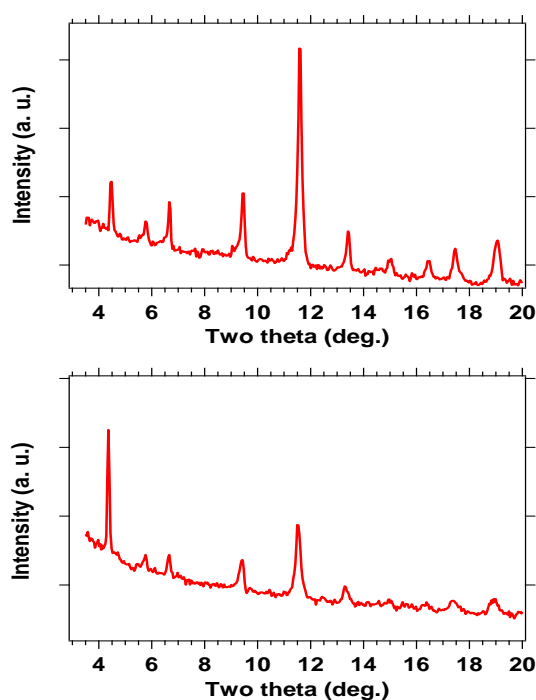
1.MOF structural characterization

Figure S1: XRD data for HKUST-1 before and after infiltration with TCNQ.

2. Channel length dependence of conductivity

We measured the I-V characteristics at different temperatures for several devices fabricated with the $TCNQ@Cu_3(BTC)_2$ thin film presented in the main text. These devices had channel lengths varying between 85 and 160 microns. In all cases we found linear I-V characteristics, and the extracted resistance as a function of channel length is shown in Fig. S2. The linear scaling with channel length shows that the resistance is dominated by transport in the thin film, as opposed to contact resistance.
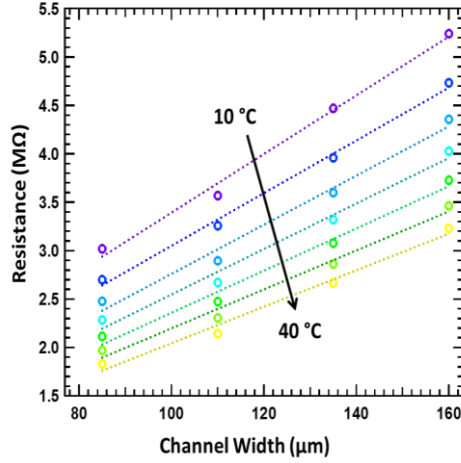
Figure S2: Resistance as a function of the separation between contacts measured at 7 different temperatures.

3. TDTR measurements of thermal conductivity and heat capacity

In TDTR, the time evolution of the surface temperature is measured through the temperature dependent changes in reflectivity (i.e., the thermoreflectance).[1] In our TDTR experimental setup, laser pulses emanate from a Ti:Sapphire oscillator with an 80 MHz repetition rate and are energetically split into pump and probe paths.[2] The train of ultra-short pump pulses thermally stimulate the Al metal dots (we confirm the thickness of each dot used in our TDTR measurements with mechanical profilometry) and time delayed probe pulses measure the change in the thermoreflectance of the sample due to the decay of the deposited thermal energy. Using lock-in amplification, we analyze the ratio of the in-phase $V_{in}(t)$ and out-of-phase $V_{out}(t)$ variations in the intensity of the reflected probe beam at the modulation frequency, f, of the pump beam as a function of delay time between the pump and probe (up to 5.5 ns). To ensure negligible sensitivity to in-plane transport, our pump and probe spot sizes were focused to $1/e^2$ radii values of 27.5 and 11 μm, respectively.[1, 3, 4] We note that TDTR has been used extensively to measure the thermal conductivity of thermally insulative thin films,[5-9] validating our approach.

TDTR experimental details and analysis are well documented in the literature,[1, 2] and only the pertinent and unique aspects of our specific experiments are discussed here, specifically, sensitivity calculations of our measurements to the thermal conductivity of the TCNQ@Cu$_3$(BTC)$_2$ MOF film. The Al metal dots were used for TDTR transduction, the thicknesses of which were verified with profilometry as 220 nm. We analyze the TDTR data in Fig. 4a of the main document using a model that accounts for diffusion through the Al film, the TCNQ@Cu$_3$(BTC)$_2$ MOF film, the 100 nm thermal oxide and the semi-infinite Si substrate. To determine the thermal conductivity of the TCNQ@Cu$_3$(BTC)$_2$ MOF film, all other thermophysical properties of each material and interface in the sample must be known. Where heat capacities and thermal conductivities of the Al, SiO$_2$ and Si are well documented in the literature (including reduced thermal conductivities of typical Al films used in TDTR measurements),[3, 10-13] both the heat capacity and thermal conductivity of the TCNQ@Cu$_3$(BTC)$_2$ MOF film and thermal boundary conductance across the MOF-adjacent interfaces are unknowns in our analysis. To alleviate this, we conduct TDTR measurements at a pump frequency of f = 1.034 MHz, which provides robust sensitivity to the thermal conductivity of the MOF (κ_{MOF}) while a relatively low sensitivity to the heat capacity of the MOF (C_{MOF}) and thermal conductances across the Al/MOF and MOF/SiO$_2$ interfaces ($h_{K,Al/MOF}$ and $h_{K,MOF/SiO2}$, respectively). This is quantified in Figure S4a, which shows the sensitivity of the TDTR signal (ratio of in-phase to out-of-phase voltages recorded by the lock-in amplifier, $-V_{in}(t)/-V_{out}(t)$) to various thermophysical properties in the sample x, where x denotes κ_{MOF}, C_{MOF}, $h_{K,Al/MOF}$ or $h_{K,MOF/SiO2}$. This TDTR sensitivity, S_x, is calculated by

$$S_x(t) = \frac{\partial \ln\left[-\dfrac{V_{in}(t)}{V_{out}(t)} \right]}{\partial \ln[x]} \qquad (S1)$$

where t is the pump-probe delay time. At a pump frequency of f = 1.034 MHz, our thermal signal is dominated by the thermal conductivity of the TCNQ@Cu$_3$(BTC)$_2$ MOF film. The

sensitivity of our TDTR measurements at $f = 1.034$ MHz to κ_{MOF} is roughly an order of magnitude greater than C_{MOF} over nearly the entire pump-probe delay time.

Even with this dominant sensitivity to κ_{MOF} at $f = 1.034$ MHz, we further reduce the uncertainty to κ_{MOF} by determining C_{MOF} through TDTR measurements at $f = 8.8$ MHz. By changing the pump modulation frequency, we vary the depth under the surface that is thermally probed during a TDTR experiment, and thereby vary the sensitivity of our measurement to C_{MOF}.[6, 14] As discussed above and quantified in Figure S3a, at 1.034 MHz our measurements are most sensitive to the thermal conductivity of the MOF more so than any other thermophysical property in the measurement volume; therefore, at this frequency, we fit our TDTR model to our data by only adjusting the thermal conductivity of the TCNQ@Cu$_3$(BTC)$_2$ MOF, yielding relatively low uncertainty in our thermal conductivity measurements. Due to the relatively low thermal conductivity of the MOF, we are insensitive to the thermal boundary conductances at each interface, and at 8.8 MHz, we are most and nearly equally sensitive to both the thermal conductivity and heat capacity of the MOF sample, as quantified via calculations of Equation S1 in Figure S4b. Therefore, we use the measured value for thermal conductivity at 1.034 MHz as input for our analysis at 8.8 MHz, leaving the only free parameter for analysis at this 8.8 MHz as the heat capacity. Therefore, using these two pump modulation frequencies, we determine the thermal conductivity and heat capacity of the TCNQ@Cu$_3$(BTC)$_2$ MOF film by iterating our TDTR fitting analysis between these two frequencies. With this dual frequency analysis, we determine that for our TCNQ@Cu$_3$(BTC)$_2$ MOF film, $C_{MOF} = 1.20\pm0.13$ MJ m^{-3} K^{-1} and $\kappa_{MOF} = 0.27\pm 0.04$ W m^{-1} K^{-1}. The heat capacity obtained from our TDTR measurements is within 25% of the Dulong-Petit (upper) limit (1.6 MJ MJ m^{-3} K^{-1} calculated using a density of 63.9 mol/L based on 1 TCNQ per MOF unit cell).
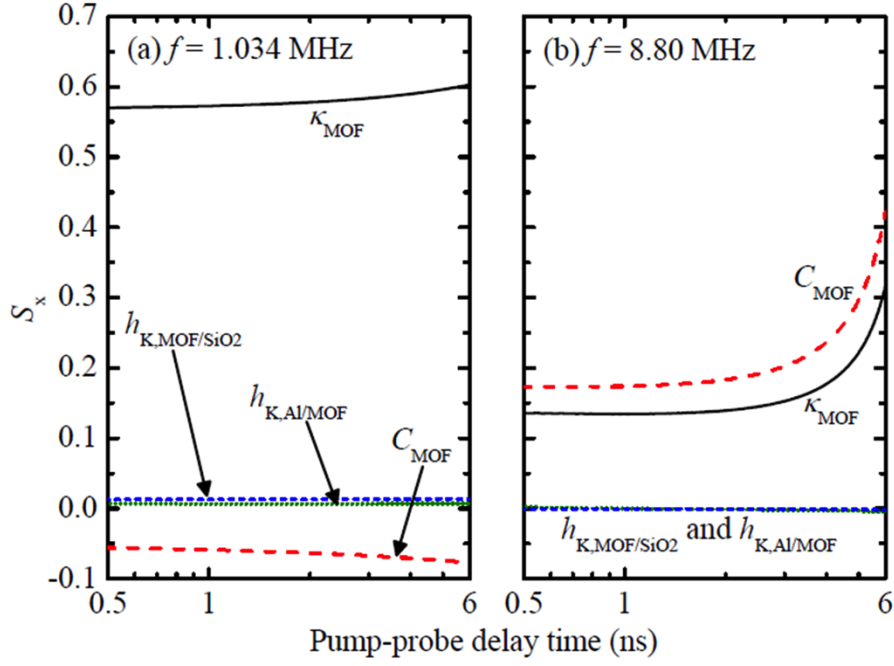
Figure S3. Sensitivities of the TDTR signal (ratio of in-phase to out-of-phase voltages recorded by the lock-in amplifier, $-V_{in}(t)/-V_{out}(t)$) to various thermophysical properties in the sample x, where x denotes κ_{MOF}, C_{MOF}, $h_{K,Al/MOF}$ or $h_{K,MOF/SiO2}$. These sensitivities were calculated via Eq. S1 assuming a pump modulation frequency of (a) $f = 1.034$ MHz and (b) $f = 8.80$ MHz.

4. Molecular dynamics simulations of thermal conductivity

The Green-Kubo method uses the auto-correlation of equilibrium heat flux J to calculate the conductivity κ from the expression

$$\kappa = \frac{V}{k_B T^2} \int_0^\infty \langle J(0) \cdot J(t) \rangle dt \tag{2}$$

where V is the system volume, T is the temperature, k_B is the Boltzmann constant, $\langle \cdot \rangle$ denotes the canonical ensemble average, and $\langle J \rangle = 0$ in equilibrium. The microscopic definition of the heat flux in terms of the phase space of the molecular system can be found in Ref.[15] and includes contributions from all forms of interatomic forces: covalent bonds, short-range

Lennard-Jones interactions and Coulombic forces. The CVFF[16] and AMBER[17] parameterization were used to represent the HKUST and TCNQ molecules, respectively. The AMBER parameterization was also used to represent the intermolecular forces, e.g., the Cu-N bonding between HKUST and TCNQ.

We employed 2x2x2 super-cells to minimize the finite size effects based on the work of Huang et al. which calculated the MOF-5 thermal conductivity[18]. To ensure that the canonical ensemble was sampled sufficiently, 5-10 replicas derived from different starting velocities and run for 1 ns where averaged to form the time-correlation of the heat flux. To validate our calculation method and choice of potential, we computed the thermal conductivity of MOF-5, obtaining $\kappa = 0.25 \pm 0.03$ W/m-K. This is in good agreement with the value $\kappa = 0.31 \pm 0.02$ W/m-K calculated in Ref.[18] and confirmed by experiment in Ref [19].

We also examined the dynamics of the system with TCNQs which interacted with MOF framework through non-bonded interactions. Consistent with the enhancement of the thermal conductivity it appeared that the TCNQs provided structured additions to the MOF framework and where also more closely bound to one of the two Cu pairs that comprised the TNCQ N to HKUST Cu bond as in Ref. 8.

References

[1] D. G. Cahill. *Rev. Sci. Instrum.* **2004,** *75*, 5119.
[2] P. E. Hopkins. *ISRN Mech. Eng.* **2013,** *2013*, 682586.
[3] P. E. Hopkins, J. R. Serrano, L. M. Phinney, S. P. Kearney, T. W. Grasser, C. T. Harris. *J. Heat transfer* **2010,** *132*, 081302.
[4] A. J. Schmidt, X. Chen, G. Chen. *Rev. Sci. Instrum.* **2008,** *79*.
[5] J. C. Duda, P. E. Hopkins, Y. Shen, M. C. Gupta. *Phys. Rev. Lett.* **2013,** *110*, 015902.
[6] X. Wang, C. D. Liman, N. D. Treat, M. L. Chabinyc, D. G. Cahill. *Phys. Rev. B* **2013,** *88*, 075310.
[7] J. C. Duda, P. E. Hopkins, Y. Shen, M. C. Gupta. *Appl. Phys. Lett.* **2013,** *102*.
[8] J. Liu, B. Yoon, E. Kuhlmann, M. Tian, J. Zhu, S. M. George, Y.-C. Lee, R. Yang. *Nano Lett.* **2013,** *13*, 5594.
[9] B. M. Foley, H. J. Brown-Shaklee, M. J. Campion, D. L. Medlin, P. G. Clem, J. F. Ihlefeld, P. E. Hopkins. *J. Am. Ceram. Soc.* **2014,** *98*, 624.

[10] C. Y. Ho, *Thermal conductivity of the elements : a comprehensive review*. American Chemical Society, Washington, **1975**.

[11] Y. S. Touloukian, R. W. Powell, C. Y. Ho, P. G. Klemens, *Thermophysical Properties of Matter - Specific Heat: Nonmetallic Solids*. IFI/Plenum, New York, **1970**.

[12] Y. S. Touloukian, R. W. Powell, C. Y. Ho, P. G. Klemens, *Thermophysical Properties of Matter - Thermal Conductivity: Nonmetallic Solids*. IFI/Plenum, New York, **1970**.

[13] J. P. Feser, D. G. Cahill. *Rev. Sci. Instrum.* **2012,** *83*.

[14] J. Liu, J. Zhu, M. Tian, X. Gu, A. Schmidt, R. Yang. *Rev. Sci. Instrum.* **2013,** *84*.

[15] J. H. Irving, J. G. Kirkwood. *J. Chem. Phys.* **1950,** *18*, 817.

[16] L. Zhao, Q. Yang, Q. Ma, C. Zhong, J. Mi, D. Liu. *J Mol Model* **2011,** *17*, 227.

[17] J. Wang, R. M. Wolf, J. W. Caldwell, P. A. Kollman, D. A. Case. *J. Comput. Chem.* **2004,** *25*, 1157.

[18] B. L. Huang, A. J. H. McGaughey, M. Kaviany. *Int. J. Heat Mass Transfer* **2007,** *50*, 393.

[19] B. L. Huang, Z. Ni, A. Millward, A. J. H. McGaughey, C. Uher, M. Kaviany, O. Yaghi. *Int. J. Heat Mass Transfer* **2007,** *50*, 405.